J. Mech. Phys. Solids 191 (2024) 105760

Contents lists available at ScienceDirect

Journal of the Mechanics and Physics of Solids

journal homepage: www.elsevier.com/locate/jmps

Ductility of a nanocomposite of glassy and rubbery polymers

Christine Heera Ahn, Guogao Zhang, Zhigang Suo *

John A. Paulson School of Engineering and Applied Sciences, Harvard University, MA 02138, United States

ARTICLE INFO

Keywords:
Interpenetrating polymer network
Poly(methyl methacrylate)
Poly(ethyl acrylate)
Ductility

ABSTRACT

A brittle glassy polymer can be made ductile by forming a nanocomposite with a rubbery polymer. This paper investigates a nanocomposite of poly(methyl methacrylate) (PMMA) and poly (ethyl acrylate) (PEA). Pure PMMA is a brittle glass, pure PEA is a rubber, and a PEA-PMMA nanocomposite is ductile. We fabricate the nanocomposite by swelling PEA with MMA monomer, followed by polymerizing MMA. We prepare nanocomposites of various weight fractions of PMMA and measure their properties, including modulus, yield strength, fracture strain, fracture strength, work of fracture, and toughness. Whereas bulk PMMA fractures at a strain of ~0.05 by localizing inelastic deformation in crazes, the PEA-PMMA nanocomposite can be stretched several times its original length with homogeneous deformation. The nanocomposite separates into a glassy phase and a rubbery phase. For a nanocomposite of 45 % weight fraction of PMMA, atomic force microscopy shows that the two phases are bicontinuous and the phase size is at ~20 nm. For the nanocomposite to undergo large deformation, the continuous glassy phase must accommodate. Our experiments exclude the mechanism that the glassy phase in the nanocomposite breaks into small pieces. Rather, the glassy phase in the nanocomposite is itself ductile. We discuss the molecular picture of this ductility.

1. Introduction

Some brittle glassy polymers become ductile when they form nanocomposites with rubbery polymers. For example, at room temperature, poly(methyl methacrylate) (PMMA) is a brittle glassy polymer of a rupture strain of ~0.05, and poly(ethyl acrylate) (PEA) is a rubbery polymer that can be stretched several times its original length. A nanocomposite of PMMA and PEA can also be stretched several times its original length (Adachi and Kotaka, 1982). Similar observations have been made in nanocomposites of other pairs of glassy and rubbery polymers, including PMMA-polyurethane (Hur et al., 1990; Jajam et al., 2013), PMMA-styrene-butadiene (James et al., 2021), PMMA-poly(acrylic acid) hydrogel (Zhang et al., 2022), polystyrene-natural rubber (Mathew et al., 2001), and PMMA-epoxy (Ratna et al., 2021).

In each of these examples, the glassy polymer forms a continuous phase, rather than individual particles. Consequently, the large rupture strain of the nanocomposite requires the glassy phase to accommodate the deformation. The mechanism of this ductility has remained uncertain. Here we examine two potential mechanisms of large deformation in such a nanocomposite. First, upon being stretched, the glassy polymer breaks into small pieces, and the nanocomposite behaves like a particle-reinforced elastomer. Second, in the nanocomposite, the glassy polymer becomes itself ductile.

We examine these potential mechanisms using PEA-PMMA nanocomposites as a model system. We fabricate such nanocomposites

* Corresponding author.
E-mail address: suo@seas.harvard.edu (Z. Suo).

https://doi.org/10.1016/j.jmps.2024.105760
Received 16 January 2024; Received in revised form 5 April 2024; Accepted 30 June 2024
Available online 1 July 2024

by swelling PEA with MMA monomer, followed by polymerizing MMA. We prepare nanocomposites of various weight fractions of PMMA and measure their properties, including modulus, yield strength, fracture strain, fracture strength, work of fracture, and toughness. Bulk PMMA fractures at a small strain of ~0.05 by localizing inelastic deformation in crazes. By contrast, the PEA-PMMA nanocomposite can be stretched several times its original length by homogeneous deformation. We subject the nanocomposite to loading and unloading, followed by heating the nanocomposite at 140°C for three minutes. When cooled back to room temperature, the nanocomposite recovers the initial shape, and the stress-strain curve is indistinguishable from that of the original nanocomposite. We further subject the nanocomposite to a succession of loops of loading, unloading, and reloading with an increasing strain for each loop. The modulus measured at each unloading increases with the number of loops. Taken together, these observations exclude the mechanism that the glassy phase in the nanocomposite breaks into small pieces. Rather, the glassy phase in the nanocomposite is itself ductile. We discuss the molecular picture of this ductility.

The ductile behavior of PEA-PMMA nanocomposites has been reported before (Adachi and Kotaka, 1982). Their study focuses on how bicontinuous structures develop during synthesis. They measure storage and loss moduli, as well as stress-strain curves. Here we further measure fracture toughness and work of fracture, load and unload samples to characterize damage, make microscopic observations of phases, and discuss the origin of ductility. Furthermore, we show how the fractocohesive length varies with the weight fraction of PMMA.

2. Preparation of PEA-PMMA nanocomposites

We prepare the PEA-PMMA nanocomposite as follows. All chemicals were purchased and used without any modification. A PEA precursor is prepared by mixing ethyl acrylate (EA, Sigma Aldrich, E9706) monomer with crosslinker N,N'-Methylenebisacrylamide (MBAA, Sigma Aldrich, M7279) and photoinitiator 2-Hydroxy-4'-(2-hydroxyethoxy)-2-methylpropiophenone (Irgacure 2959, Sigma Aldrich, 410896) (Fig. 1A). The crosslinker-to-monomer molar ratio is 10^{-4}, and the initiator-to-monomer molar ratio is 0.4. The precursor is poured into a mold made of a glass plate and a silicone spacer (McMaster, 1460N11). The mold is then covered with another glass plate, and the two glass plates are clipped using binder clips. The sample clipped between the glass plates is then placed in a polyethylene bag (VWR, 4662002). The mixture is polymerized under ultraviolet irradiation (15W 265nm; UVP XX-15L) for 12 h (Fig. 1B). The prepared PEA film has a thickness of ~0.7 mm. The sample is taken out of the polyethylene bag, and placed in a hood for 12 h to evaporate unreacted monomers.

A PMMA precursor is prepared by mixing methyl methacrylate (MMA, Sigma Aldrich, M55909) monomer, MBAA crosslinker, and Irgacure 2959 photoinitiator (Fig. 1C). The crosslinker-to-monomer molar ratio is 10^{-4}, and the initiator-to-monomer molar ratio is 0.4. The PEA film is then submerged in the PMMA precursor to swell for a certain amount of time (Fig. 1D). The sample is taken out of the PMMA precursor, and the PMMA precursor on the surface is wiped off. The ratio of the weight of the swollen film to that of the pristine film, w/w_0, increases with time of submersion, and plateaus at $w/w_0 \sim 7$ after one hour (Fig. 2). Denote the weight fraction of PMMA by $\varphi = (w/w_0) - 1$. Further denote a nanocomposite of weight fraction of, for example, $\varphi = 45$ %, by PEA-PMMA_{45}.

Each PEA-MMA film is placed between two glass plates, and then in a polyethylene bag sealed with vacuum sealer to remove air and prevent evaporation of MMA. Then the two glass plates are fixed with binder clips. The films are stored overnight to homogenize the PMMA precursor in the PEA film (Fig. 1E). The MMA monomer is polymerized under ultraviolet irradiation to obtain a PEA-PMMA nanocomposite (Fig. 1F). The nanocomposite is taken out of the polyethylene bag and is placed in a hood for 24 h to evaporate unreacted monomers.

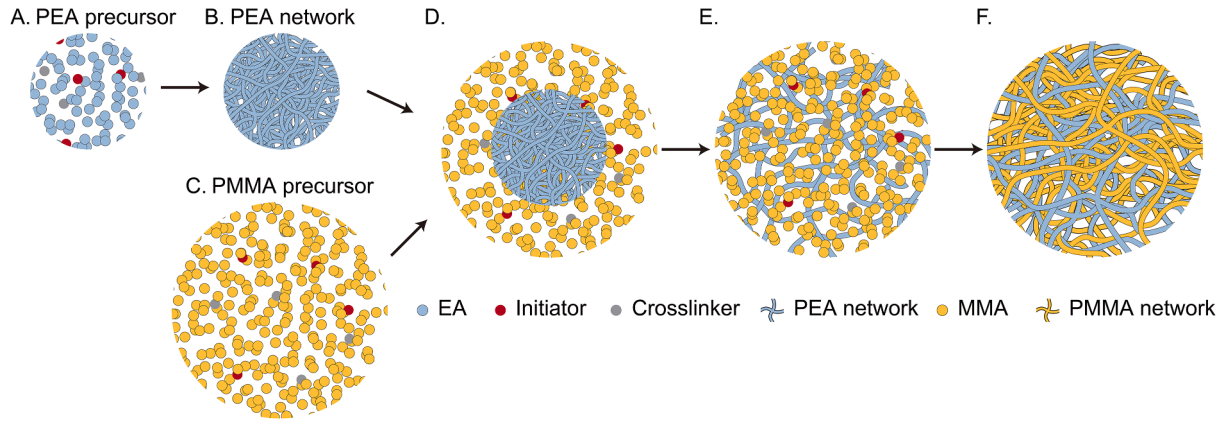

Fig. 1. Preparation of a PEA-PMMA nanocomposite. (A) The PEA precursor is composed of EA monomer, MBAA crosslinker, and Irgacure 2959 initiator. (B) The PEA network is formed under ultraviolet irradiation. (C) The PMMA precursor is composed of MMA monomer, MBAA crosslinker, and Irgacure 2959 initiator. (D) The PEA network is submerged in the PMMA precursor to swell for a certain time. (E) The sample is taken out of the PMMA precursor, and then the PMMA precursor in the PEA network is homogenized. (F) The PMMA network is formed under ultraviolet irradiation.

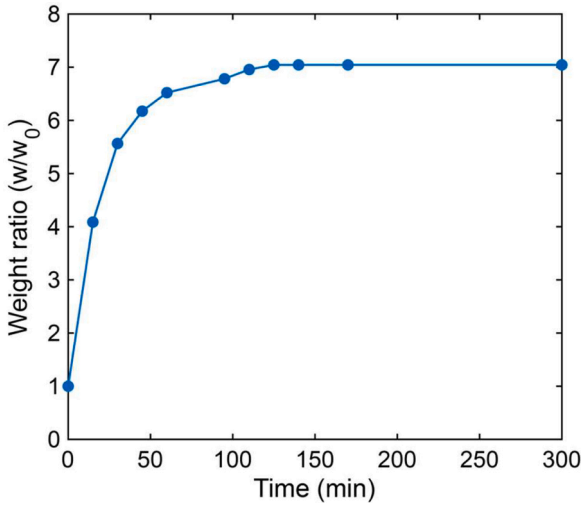

Fig. 2. Submerged in the PMMA precursor at room temperature, the PEA film swells and gains weight over time.

3. Mechanical properties

We conduct uniaxial tensile tests for nanocomposites of various PMMA weight fractions. From a film of each weight fraction, we use a laser cutter (Helix 75 W, Epilog Laser) to cut three dogbone-shaped specimens, with gauge length 12 mm and width 2 mm, following the ISO 527-2-5B standard. For each weight fraction, three films are fabricated, and a total of nine specimens are subjected to the tensile test. Each specimen is tested by a tensile tester (Instron; 5966) with a 10 kN load cell. The specimen is stretched monotonically at a velocity of 0.1 mm/s until break, while the force and displacement are recorded. Nominal stress is defined as the force divided by the cross-sectional area of the undeformed specimen. Strain is defined as the displacement of the crosshead of the tensile machine divided by the gauge length of the undeformed specimen. To ascertain the accuracy of the procedure, we have also marked two points at the end of the gauge length of a specimen, videotaped the tensile test, and calculated the strain as the displacement between the two markers divided by the undeformed gauge length. The strains obtained by the two procedures are nearly identical. In this paper, we report all strains determined by the first procedure.

When bulk PMMA is pulled, inelastic deformation localizes to form crazes (Fig. 3A). Outside the crazes, the bulk PMMA is nearly elastic and has a low strain of ~0.05. Bulk PMMA only forms one or a few crazes, so that the macroscopic strain at rupture is ~0.05. By contrast, the PEA-$PMMA_{45}$ nanocomposite delocalizes inelastic deformation. Even at a large strain of 3, the sample deforms homogeneously, without any crazes (Fig. 3B).

For each PMMA weight fraction φ, we plot stress-strain curves of the nine specimens (Fig. 4). For pure PMMA, $\varphi = 100$ %, as the strain increases, the stress rises, peaks, and drops. The specimen fractures without appreciable inelastic deformation. For each PEA-PMMA nanocomposite tested, as the strain increases, the stress rises, peaks, drops, and increases again. Here, we observe localized

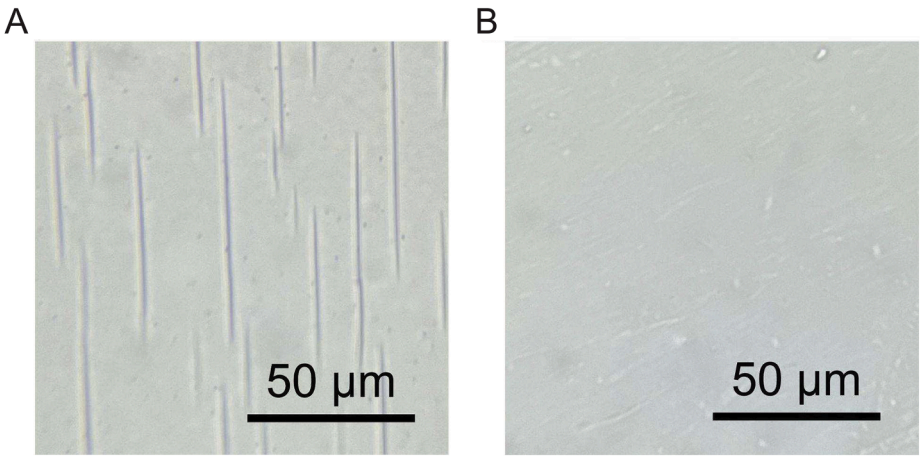

Fig. 3. Optical images of samples after deformation. (A) Bulk PMMA at a strain of 0.04 forms crazes. (B) The PEA-$PMMA_{45}$ nanocomposite at a strain of 3 deforms homogeneously.

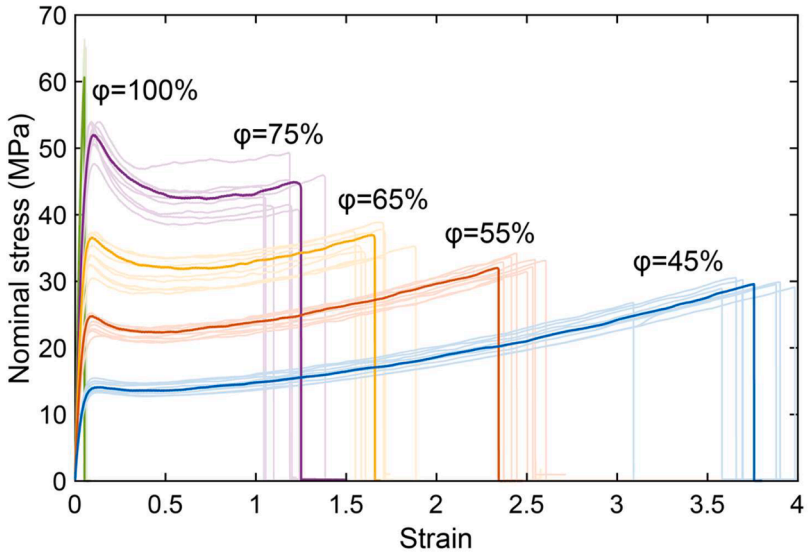

Fig. 4. Stress-strain curves of specimens of various PMMA weight fractions φ. For each composition, nine specimens are tested.

deformation in the nanocomposites. After initial localization, the deformation within the localized region becomes stable, but the localized region starts to propagate throughout the length of the sample. A similar observation is also reported in the literature (Adachi and Kotaka, 1982).The specimen fractures after extensive inelastic deformation.

From each stress-strain curve, we determine five properties: modulus, yield strength, fracture strength, fracture strain, and work of fracture (Fig. 5). The modulus is determined by the difference in stress divided by the difference in strain between 0.0005 and 0.0025. Pure PMMA does not have appreciable inelastic deformation, so that the yield strength is not reported. For each nanocomposite specimen, the yield strength is taken to be the peak stress. The work of fracture W_c is the area under the stress-strain curve up to the fracture strain. In this study, we are interested in ductility of materials of high modulus, comparable to those of thermoplastics. Thus,

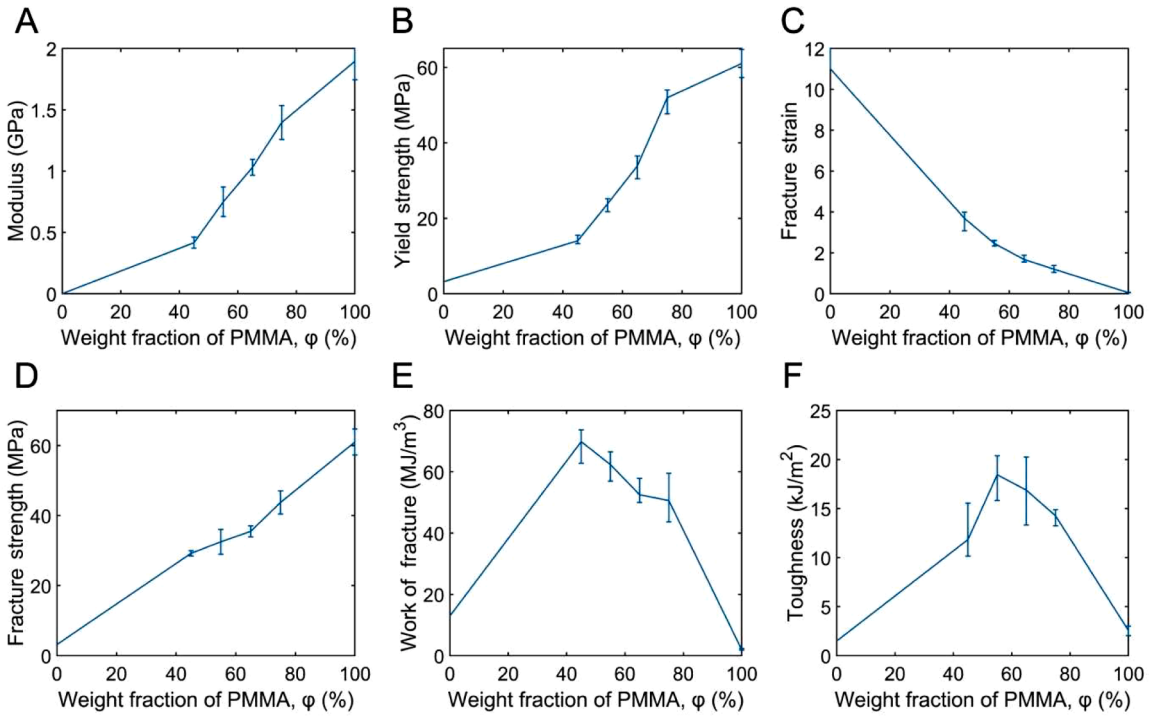

Fig. 5. Properties of specimens of various PMMA weight fractions φ. (A) Modulus, (B) Yield strength, (C) Fracture strain, (D) Fracture Strength, (E) Work of fracture, (F) Toughness.

we focus on nanocomposites of high weight fraction of PMMA. If the weight fraction of PMMA is too low, the PMMA phase will no longer be continuous, so that the modulus will be low. We report data for nanocomposites of the weight fraction of PMMA above 45 %. Note that we conduct experiments for φ= 0, 45, 55, 65, 75, and 100 %. For the other weight fractions, there are no experimental data available. The straight lines are used to guide the eye.

We measure toughness using the single-edge notch test. We use the laser cutter to cut from a film a specimen of a rectangular shape, height 55 mm and width 21 mm. We then use a razor blade to introduce a precut of ~6 mm at the middle of the height. After gripping the specimen on the Instron, the testing area of the specimen is 40 mm high and 21 mm wide. The specimen is monotonically stretched with a 10 kN load cell on the Instron 5966 tensile tester until the specimen fractures. The critical nominal stress σ_c is determined by the peak force divided cross-sectional area of the entire specimen. The toughness G_c is given by Tada et al. (2000):

$$G_c = \pi\sigma_c^2 a \Big/ E \left[1.122 - 0.231\ (a/b)\ + 10.55\ (a/b)^2 - 21.71\ (a/b)^3 + 30.382\ (a/b)^4\right]^2 \tag{1}$$

where a is the precut length, b is the width of the specimen, and E is the modulus. For each weight fraction of PMMA, six specimens are tested.

Under the small scale yielding conditions, the plastic zone size R_p is estimated by Irwin (1957):

$$R_p = \frac{G_c E}{2\pi\sigma_Y{}^2} \tag{2}$$

where σ_Y is the yield strength. The plastic zone size for each composition is estimated as follows: 3.98 mm for PEA-PMMA$_{45}$, 3.89 mm for PEA-PMMA$_{55}$, 2.41 mm for PEA-PMMA$_{65}$, 1.23 mm for PEA-PMMA$_{75}$, and 0.23 mm for PEA-PMMA$_{100}$. For the single-edge notch test, the width of the sample is 21 mm, and the crack length is 6 mm. Although the estimated plastic zone size is smaller than the crack size for every composition, the plastic zone size is not small enough to satisfy the small scale yielding condition. Consequently, the values of toughness listed here should not be taken quantitatively. Rather, these values are listed for qualitative comparison.

The modulus is ~600 kPa for pure PEA rubber, and ~1.9 GPa for pure PMMA glass. The modulus ranges from 500 MPa to 1.4 GPa for the nanocomposites tested (Fig. 5A). The much higher modulus of each nanocomposite than pure PEA indicates that, in the nanocomposite, the PMMA phase is continuous. The moduli of the nanocomposites are nearly linear in the weight fraction of PMMA, approximately following the rule of mixture.

The yield strength is also nearly linear in the weight fraction of PMMA, approximately following the rule of mixture (Fig. 5B). Here we include the fracture strength of pure PEA and pure PMMA, even though neither is expected to yield.

As the weight fraction of PMMA increases, the fracture strain of the nanocomposite decreases (Fig. 5C). Pure PMMA is brittle and has a fracture strain of ~0.05. By contrast, the PEA-PMMA$_{45}$ nanocomposite is ductile and has a fracture strain of ~3.7. We will discuss the origin of this ductility later in the paper.

The rule of mixture also approximately holds for the fracture strength (Fig. 5D). Observe that the fracture strength of a nanocomposite is much higher than the fracture strength of pure PEA, so that the fracture strength of the nanocomposite mainly comes from the PMMA phase. The rule of mixture suggests that, in the nanocomposites, the yield strength and fracture strength of the PMMA phase are nearly independent of the weight fraction of PMMA.

The work of fracture is not monotonic as the weight fraction of PMMA increases, being ~12 MJm^{-3} for pure PEA, ~2 MJm^{-3} for pure PMMA, and ~69 MJm^{-3} for the PEA-PMMA$_{45}$ nanocomposite (Fig. 5E). This non-monotonic trend is understood as follows. Before fracture, pure PEA rubber undergoes homogeneous deformation, but pure PMMA glass undergoes localized deformation of crazes (Donald and Kramer, 1982; Kramer, 1983). Even though the work of fracture of an individual fibril in the crazes is large, the bulk of PMMA remains elastic and has a small strain, contributing negligibly to the work fracture. The presence of PEA delocalizes the inelastic deformation of PMMA throughout the nanocomposites, such that work of fracture peaks for the nanocomposites.

The toughness is also not monotonic as the weight fraction of PMMA increases, being ~1,500 Jm^{-2} for pure PEA, ~2,500 Jm^{-2} for pure PMMA, and ~18,500 Jm^{-2} for the PEA-PMMA$_{55}$ nanocomposite (Fig. 5F). Pure PEA has modest hysteresis, so that its toughness comes from the synergy of the modest hysteresis in the bulk and the scission of polymer chains on the crack plane (Kim et al., 2021). Pure PMMA has negligible hysteresis, and its toughness comes almost exclusively from the formation and rupture of fibrils in crazes (Brown, 1991). By contrast, in a PEA-PMMA nanocomposite, the inelastic deformation of PMMA is delocalized throughout the sample, such that toughness comes from the synergy of the rupture of PMMA at the crack plane and the inelastic deformation in the bulk.

For a given material, each property is a random variable. We characterize its statistical scatter by the coefficient of variation (COV), defined by the standard deviation divided by the average. The COV is dimensionless and can be used to compare the scatters of various properties. The COV of every one of the six properties is smaller than ~17 % (Fig. 6).

The similar statistical scatters of all six properties are appreciated when we compare them to those of silica. For silica, fracture strength scatters much more than toughness and modulus. This difference is attributed to the fact that silica is extremely flaw-sensitive. A crack-like flaw longer than nanometers can concentrate stress and knock down fracture strength (Proctor et al., 1967; Griffith and Taylor, 1921). Fractocohesive length is defined by the toughness divided by the work of fracture (G_c/W_c) (Chen et al., 2017). For silica, the fractocohesive length is ~1 nm. By contrast, the fractocohesive lengths for PMMA, PEA, and PMMA-PEA are large (Fig. 7). Because the COV is small for all properties, for a nanocomposite of a given PMMA weight fraction, we calculate the fractocohesive length G_c/W_c by the ratio of the average G_c to the average W_c. Observe that the fractocohesive length is large for pure PMMA because it has a small value of the work of fracture (Fig. 5E).

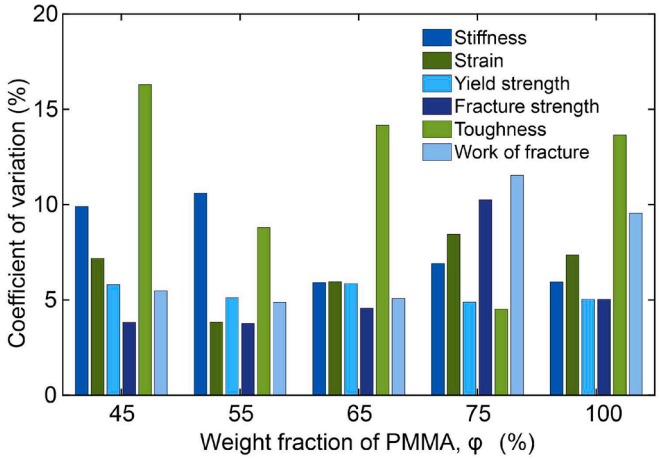

Fig. 6. Coefficients of variation for six properties of PEA-PMMA nanocomposites of five PMMA weight fractions.

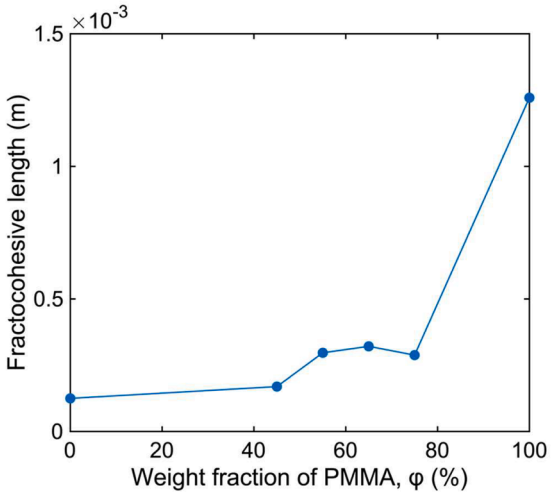

Fig. 7. Fractocohesive length G_c/W_c as a function of PMMA weight fraction.

4. Atomic force microscopy

Pure PMMA has a modulus of ~1.9 GPa and a fracture strain of ~0.05. The PEA-$PMMA_{45}$ composite has a modulus of ~0.415 GPa and a fracture strain of ~3.7. Because pure PEA has a modulus of ~600 kPa, the high modulus of the nanocomposite indicates that the PMMA in the nanocomposite is continuous and bears most of the load. We use atomic force microscopy (AFM) to confirm the morphology of the phases in the PEA-PMMA composite (Fig. 8). The PEA is cut into a small piece and swollen to a target weight fraction of PMMA, $\varphi = 45$ %. The PEA-MMA_{45} composite is then placed on top of the cleaned wafer (University Wafer) to minimize roughness of the surface. Then, the sample is sandwiched between two glass plates and sealed in a polyethylene bag to prevent the MMA monomer from evaporating. The sample is homogenized overnight and polymerized under ultraviolet irradiation. The obtained PEA-PMMA nanocomposite is detached from the wafer, and the surface is imaged using an AFM (Asylum Research) in ambient air.

A PEA-PMMA nanocomposite separates into two phases: a PEA-rich phase and a PMMA-rich phase. The two dissimilar polymers have energy of mixing, which drives the two polymers to separate into phases. The two dissimilar polymers also have entropy of mixing, which drives the two polymers to mix. The energy of mixing is independent of the length of the polymers, but the entropy of mixing decreases as the length of the polymers increases. The MMA monomers and the PEA polymers have a large entropy of mixing, which drives the MMA monomers to swell the PEA network. After polymerization of the MMA monomers, the low entropy of mixing of the two polymers PMMA and PEA drives them to separate into two phases.

As we noted above, the polymer-polymer mixture does separate into phases. Before the MMA monomers polymerize, the PEA chains are crosslinked into a continuous network. The monomer-polymer mixture does not separate into two phases, but forms a gel. When the MMA monomers start to polymerize, numerous regions of the PMMA-rich phase nucleate. As more MMA monomers polymerize, these regions of the PMMA-rich phase grow. In a later stage of polymerization, the regions of PMMA-rich phase percolate,

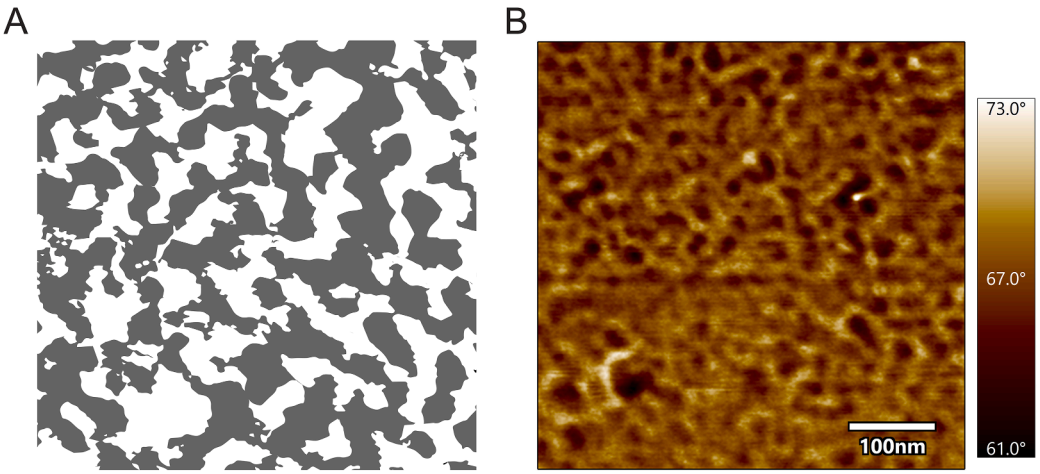

Fig. 8. (A) Schematic of a nanocomposite of bicontinuous phases. (B) Atomic force microscope image of bicontinuous phases in a PEA-PMMA$_{45}$ nanocomposite. The darker brown and black regions belong to the PMMA-rich phase. The lighter brown and white regions belong to the PEA-rich phase.

so long as the volume fraction of PMMA in the nanocomposite is larger than ~20 %. Consequently, the region of PEA-rich phase forms a continuous structure, the region of PMMA-rich phase forms another continuous structure, and the nanocomposite forms a bicontinuous structure (Fig. 8A). In the PEA-PMMA nanocomposites that we have prepared, the PEA chains form one crosslinked network, and the PMMA chains form another crosslinked network. The two networks interpenetrate, forming an interpenetrating polymer network (IPN). The topological constraint of the interpenetration, as well as the glassy structure of PMMA, immobilizes polymer chains and arrests the coarsening of the two phases.

The bicontinuous structure is confirmed by an AFM phase image of the PEA-PMMA$_{45}$ nanocomposite (Fig. 8B). The image is obtained in the tapping mode of the AFM. The cantilever of the AFM is driven to oscillate by applying an electrical signal to a piezoelectric in the holder of the cantilever. The cantilever oscillation is detected by the light reflected from the cantilever. In the tapping mode, the frequency and amplitude of the electrical signal are kept constant. When the cantilever tip dwells on a location of the sample surface, the cantilever can oscillate in a steady state, at the same frequency as that of the electrical signal. As the location of the sample surface varies, the steady state amplitude of the cantilever oscillation is controlled to be a constant by adjusting the height of the cantilever through the feedback of an electronic servo. The cantilever scans over the sample at a speed low enough to achieve steady-state oscillation of constant amplitude. The oscillation of the cantilever lags behind the oscillation of the electrical signal. This lag, coded in color, is used to form the AFM phase image. The lag depends on the viscoelasticity of the sample, as well as on the molecular interactions between the AFM tip and the sample.

The AFM tip has a diameter of ~14 nm, too large to resolve the thickness of the phase boundary, which is ~ 1 nm. The diameter of the AFM tip is comparable to the feature size of the phases. When the cantilever tip dwells at a location mainly of the PMMA phase, the lag is small and is coded in dark brown. When the cantilever tip dwells at a location mainly of the PEA phase, the lag is large and is coded in light brown. When the cantilever tip dwells at a location of partly PMMA phase and partly PEA phase, the lag is intermediate and is coded intermediate between dark and light brown. The surface of the sample also has roughness, which may also affect the AFM phase image. These complications are common in AFM imaging and will not be studied in this work. The observed feature size of the phases is ~20 nm.

5. Does deformation break the glassy phase into pieces?

We have shown above that the PEA-PMMA$_{45}$ nanocomposite can undergo much larger deformation than bulk PMMA. We have also shown that the PEA-PMMA$_{45}$ nanocomposite separates into two phases, a continuous PMMA-rich phase and a continuous PEA-rich phase. Consequently, the large deformation must be accommodated by the continuous PMMA-rich phase. Does the large deformation of the nanocomposite break the PMMA-rich phase, or deform it? To answer this question, we conduct two types of experiments.

In the first experiment, a dog-bone shaped specimen is preheated at 140°C for three minutes. The specimen is then pulled at room temperature monotonically using the tensile tester to a strain of 2.52. When the applied force is removed, the sample has a residual strain of 2.1 (Fig. 9). The specimen recovers its original shape and length by heating at 140°C for three minutes. The recovered specimen is pulled at room temperature to a strain of 2.52 again and is then unloaded. The first and second stress-strain curves of loading and unloading coincide. The experiment is repeated nine times with each time using a new sample, and for every specimen, the observations are similar as described above. Note that the strain of 2.52 is much larger than the fracture strain of bulk PMMA. These observations indicate that, after annealing, the PMMA phase recovers its original morphology and is still continuous. Because the annealing temperature is above the glass transition temperature of bulk PMMA, the mobility of the PMMA chains enables the sample to relax. This experiment by itself, however, does not show whether the tensile test has damaged PMMA, for the mobility of PMMA may also heal some damage of PMMA.

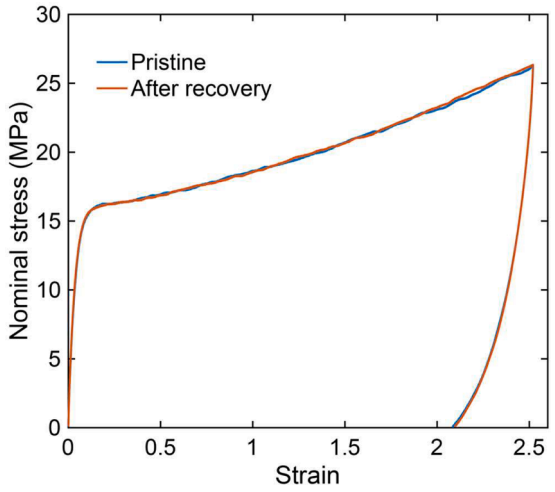

Fig. 9. Stress-strain curve of an as-prepared specimen of PEA-PMMA$_{45}$ (Blue), and of the specimen after being held at 140°C for three minutes (Red).

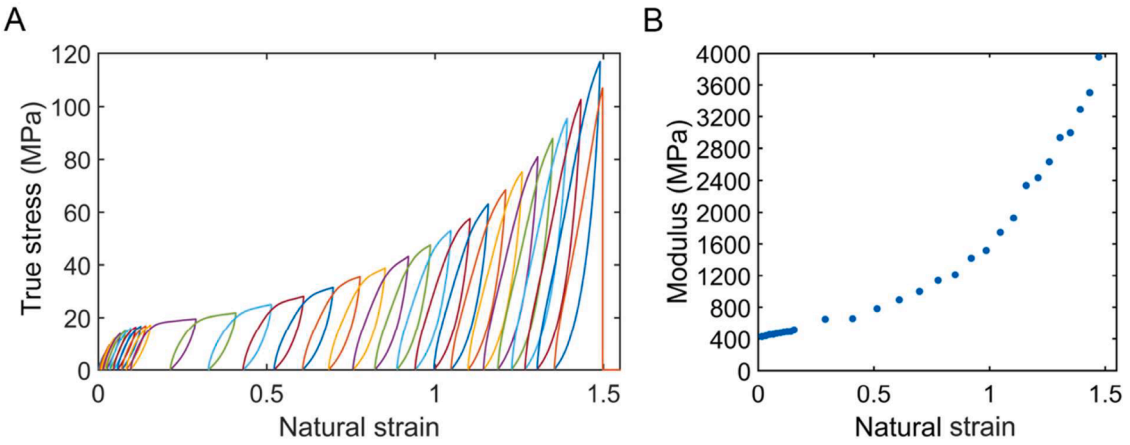

Fig. 10. (A) True stress plotted as a function of natural strain for loading, unloading, and reloading of a PEA-PMMA$_{45}$ specimen. (B) Modulus during unloading for consecutive loops.

To further ascertain if the deformation damages PMMA, we conduct a second experiment. We subject the nanocomposite to consecutive loading, unloading, and reloading, without annealing. The maximum strain increases by 0.0168 for each of the first 10 times of reloading. To prevent the sample from buckling during unloading, the unloading ends once the force reaches 0.1 N. After the first 10 times of reloading, the maximum strain increases by 0.168 each time of reloading until the sample breaks. We plot the data on the plane of true stress and natural stain (Fig. 10A). To reflect the change of cross-sectional area over the loops, we convert engineering strain to natural strain, $\varepsilon = ln(1 + L_D/L_i)$, where L_i is initial gauge length and L_D is deformed gauge length. We also convert nominal stress to true stress, $\sigma = s\,(1 + L_D/L_i)$, where s is the nominal stress. We calculate the slope at the beginning of each unloading curve. The slope increases with the number of loops, from ~400 MPa to ~4 GPa (Fig. 10B). This observation indicates that the deformation aligns the polymer chains in the PMMA phase and does not break the PMMA phase into pieces.

6. Discussion

Inelastic deformation is localized in some bulk glassy polymers but is delocalized in other bulk glassy polymers (Donald and Kramer, 1982; Kramer, 1983). The conditions for inelastic deformation to localize have long attracted attention among researchers and have remained an active area of research (Donald and Kramer, 1982; Kramer, 1983; Michler and Baltá Calleja, 2012; Wang et al., 2014). In a bulk glassy polymer, polymer chains on the surface are more mobile than those in the bulk (Sharp and Forrest, 2003; Wang et al., 2014). It is likely that this enhanced mobility of polymer chains on the surface lowers the ductile-to-brittle transition temperature, such that the polymer chains on the surface become ductile at room temperature. We surmise that the enhanced mobility of the polymer chains on the surface of a bulk polymer glass is a fundamental mechanism for ductility of materials systems that contain nanoscale polymer glasses. Here we recall several examples.

Table 1
Comparison of mechanical properties of copolymer and nanocomposite.

	Yield strength	Fracture strain	Modulus	Ultimate tensile strength	Toughness	Work of fracture
Copolymer	28.57 MPa	2.41	1.03 GPa	28.38 MPa	10911.04 Jm^{-2}	55.84 MJm^{-3}
Nanocomposite	23.83 MPa	2.46	0.75 GPa	32.51 MPa	18511.41 Jm^{-2}	62.34 MJm^{-3}

As a first example, a brittle polymer glass can form nanoscale fibrils that undergo large inelastic deformation. After a bulk polymer glass is stretched to form crazes, the inelastic deformation is localized in the crazes. Inside a craze, each fibril deforms more or less homogeneously before rupture. That is, each fibril can be considered as a ductile polymer glass. The diameter of the fibril is on the same order of magnitude as the depth of the surface layer in which the mobility of polymer chains is enhanced.

As a second example, thin freestanding PMMA films are ductile (Pantano et al., 2021). When the thickness of the PMMA film decreases from 280 nm to 180 nm, the fracture strain increases from ~0.02 to ~0.5. Similar observations have been reported for thin freestanding polystyrene films (Sato et al., 2016; Velez et al., 2020). For thin freestanding film, inelastic deformation delocalizes when the film thickness is comparable to the diameter of the craze fibrils in the bulk polymer. That is, a thin freestanding film acts like a giant fibril, deforming homogeneously.

As a third example, a laminate of a brittle polymer glass and a ductile polymer can be ductile. Similar to bulk PMMA, when bulk polystyrene is pulled, inelastic deformation localizes to form crazes, which consist of fibrils of diameter 5–18 nm (Ivan'kova et al., 2004; Michler and Baltá Calleja, 2012). The localized inelastic deformation makes bulk polystyrene brittle, which fractures at a macroscopic strain of ~0.02. Laminated polystyrene and polyethylene can be produced by coextrusion (Van Der Sanden et al., 1993). Recall that bulk polyethylene is a ductile semicrystalline polymer. When the thickness of polystyrene decreases from 35 μm to 0.8 μm, the fracture strain of the laminates increases from ~0.03 to ~0.3.

As a fourth example, a block copolymer of a glassy polymer and a rubbery polymer can be ductile (Adhikari and Michler, 2004; Michler et al., 2002). Bulk polystyrene is a glassy polymer, and bulk butadiene is a rubbery polymer. Their block copolymers of the lamellar morphology are ductile when the thickness of polystyrene layers is below a critical thickness of ~20 nm. Below the critical thickness, the fracture strain is ~2. The critical thickness is comparable to the diameter of the craze fibrils in bulk polystyrene.

As a fifth example, a random copolymer of a glassy polymer and a rubbery polymer can also be ductile (Kenney, 1968). For example, we have prepared a random copolymer of PMMA and PEA, in which the weight fraction of PMMA is 55 %. The mechanical properties of the copolymer of PMMA and PEA, are similar to the properties of the nanocomposite of this study (Table 1). We have not studied the random copolymer to the same detail as the nanocomposite.

All these examples indicate that a brittle polymer glass can be ductile when the feature size is in the nanoscale. These observations are consistent with the fact that the polymer chains on the surface of a polymer glass are more mobile than those in the bulk. It is likely that the mobility of polymer chains at the interfaces between a glassy phase and rubbery phase is also enhanced, which makes the nanocomposite ductile. This suggestion is consistent with the observation that the PEA-PMMA nanocomposite is ductile, even though bulk PMMA is brittle.

7. Concluding remarks

Bulk PMMA is a brittle glassy polymer, and bulk PEA is a rubbery polymer. This paper investigates the ductility of nanocomposites of PMMA and PEA. A PEA-$PMMA_{45}$ forms bicontinuous phases, one phase rich in PEA and the other phase rich in PMMA. The feature size of the phases is ~20 nm. Whereas bulk PMMA has a rupture strain of ~0.05, the PEA-$PMMA_{45}$ nanocomposite has a rupture strain of ~3.7. The large rupture strain of the nanocomposite requires that the PMMA-rich phase accommodate the deformation. We show that the PMMA-rich phases do not break into pieces during large deformation. Bulk PMMA ruptures by localizing inelastic deformation to form one or a few crazes consisting of fibrils. Each fibril can undergo large deformation. The bulk of PMMA outside the crazes, however, undergoes small deformation, so that the macroscopic strain at rupture is small. In the PEA-$PMMA_{45}$ nanocomposite, the feature size of the PMMA-rich phase is comparable to the diameter of the craze fibrils formed in bulk PMMA. The inelastic deformation no longer localizes, and the nanocomposite is ductile. In effect, the nanoscale PMMA-rich phase behaves like a giant fibril, capable of delocalized, large inelastic deformation. The ductility of the PEA-PMMA nanocomposite is achieved at the expense of sacrificing stiffness and strength of pure PMMA. Despite the expense, the mechanical properties of the nanocomposite are still comparable to those of commercial petroleum-derived thermoplastics, such as polyethylene. This study can potentially help the development of polymer composites of desired functions and properties. In particular, many biodegradable and bio-derived polymers do not have the mechanical properties to rival petroleum-derived polymers. This challenge may be resolved by hybridizing dissimilar biodegradable and bio-derived polymers.

CRediT authorship contribution statement

Christine Heera Ahn: Writing – review & editing, Writing – original draft, Validation, Methodology, Investigation, Formal analysis, Data curation, Conceptualization. **Guogao Zhang:** Writing – original draft, Methodology, Investigation, Formal analysis, Data curation, Conceptualization. **Zhigang Suo:** Writing – original draft, Methodology, Investigation, Formal analysis, Data curation, Conceptualization.

Declaration of competing interest

The authors declare the following financial interests/personal relationships which may be considered as potential competing interests: Christine Heera Ahn reports was provided by National Science Foundation. Zhigang Suo reports financial support was provided by Harvard University Materials Research Science and Engineering Center. Zhigang Suo reports financial support was provided by Air Force Office of Scientific Research. If there are other authors, they declare that they have no known competing financial interests or personal relationships that could have appeared to influence the work reported in this paper.

Data availability

Data will be made available on request.

Acknowledgments

This work was supported by Harvard University MRSEC (DMR-2011754) and by the Air Force Office of Scientific Research (FA9550-20-1-0397). C.H.A. was supported by the NSF Graduate Research Fellowship (DGE1745303).

References

Adachi, H., Kotaka, T., 1982. Structure and mechanical properties of sequential interpenetrating polymer networks. I. Poly(ethyl acrylate)/Poly(methyl methacrylate) system. Polym. J. 14, 379–390. https://doi.org/10.1295/polymj.14.379.

Adhikari, R., Michler, G.H., 2004. Influence of molecular architecture on morphology and micromechanical behavior of styrene/butadiene block copolymer systems. Prog. Polym. Sci. 29, 949–986. https://doi.org/10.1016/j.progpolymsci.2004.06.002.

Proctor, B.A., Whitney, I., Johnson, J.W., 1967. The strength of fused silica. Proc. R. Soc. Lond. A 297, 534–557. https://doi.org/10.1098/rspa.1967.0085.

Brown, H.R., 1991. A molecular interpretation of the toughness of glassy polymers. Macromolecules 24, 2752–2756. https://doi.org/10.1021/ma00010a018.

Chen, C., Wang, Z., Suo, Z., 2017. Flaw sensitivity of highly stretchable materials. Extreme Mech. Lett. 10, 50–57. https://doi.org/10.1016/j.eml.2016.10.002.

Donald, A.M., Kramer, E.J., 1982. The competition between shear deformation and crazing in glassy polymers. J. Mater. Sci. 17, 1871–1879. https://doi.org/10.1007/BF00540402.

Griffith, A.A., Taylor, G.I., 1921. VI. The phenomena of rupture and flow in solids. Philos. Trans. R. Soc. Lond. A 221, 163–198. https://doi.org/10.1098/rsta.1921.0006.

Hur, T., Manson, J.A., Hertzberg, R.W., Sperling, L.H., 1990. Fatigue behavior of acrylic interpenetrating polymer networks. II. J. Appl. Polym. Sci. 39, 1933–1947. https://doi.org/10.1002/app.1990.070390909.

Irwin, G.R., 1957. Analysis of stresses and strains near the end of a crack traversing a plate. J. Appl. Mech. 24, 361–364. https://doi.org/10.1115/1.4011547.

Ivan'kova, E.M., Krumova, M., Michler, G.H., Koets, P.P., 2004. Morphology and toughness of coextruded PS/PMMA multilayers. Colloid Polym. Sci. 282, 203–208. https://doi.org/10.1007/s00396-003-0906-1.

Jajam, K.C., Bird, S.A., Auad, M.L., Tippur, H.V., 2013. Tensile, fracture and impact behavior of transparent interpenetrating polymer networks with polyurethane-poly(methyl methacrylate). Polym. Test. 32, 889–900. https://doi.org/10.1016/j.polymertesting.2013.04.010.

James, J., Thomas, G.V., Rouxel, D., Strankowski, M., Kalarikkal, N., Thomas, S., 2021. Fabrication of toughened plastic using styrene butadiene rubber-poly (methyl methacrylate) interpenetrating polymer networks. Mater. Today Chem. 19, 100383 https://doi.org/10.1016/j.mtchem.2020.100383.

Kenney, J.F., 1968. Properties of block versus random copolymers. Polym. Eng. Sci. 8, 216–226. https://doi.org/10.1002/pen.760080307.

Kim, J., Zhang, G., Shi, M., Suo, Z., 2021. Fracture, fatigue, and friction of polymers in which entanglements greatly outnumber cross-links. Science 374, 212–216. https://doi.org/10.1126/science.abg6320 (1979).

Kramer, E.J., Kausch, H.H., 1983. Microscopic and molecular fundamentals of crazing. Crazing in Polymers, Advances in Polymer Science. Springer-Verlag, Berlin/Heidelberg, pp. 1–56. https://doi.org/10.1007/BFb0024055.

Mathew, A.P., Packirisamy, S., Radusch, H.J., Thomas, S., 2001. Effect of initiating system, blend ratio and crosslink density on the mechanical properties and failure topography of nano-structured full-interpenetrating polymer networks from natural rubber and polystyrene. Eur. Polym. J. 37, 1921–1934. https://doi.org/10.1016/S0014-3057(01)00067-2.

Michler, G.H., Adhikari, R., Lebek, W., Goerlitz, S., Weidisch, R., Knoll, K., 2002. Morphology and micromechanical deformation behavior of styrene/butadiene-block copolymers. I. Toughening mechanisms in asymmetric star block copolymers. J. Appl. Polym. Sci. 85, 683–700. https://doi.org/10.1002/app.10540.

Michler, G.H., Baltá Calleja, F.J., 2012. Nano- and Micromechanics of Polymers: Structure Modification and Improvement of Properties. Hanser, München.

Pantano, M.F., Pavlou, C., Pastore Carbone, M.G., Galiotis, C., Pugno, N.M., Speranza, G., 2021. Highly deformable, ultrathin large-area poly(methyl methacrylate) films. ACS Omega 6, 8308–8312. https://doi.org/10.1021/acsomega.1c00016.

Ratna, D., Dalvi, V.G., Billa, S., Sharma, S.K., Rath, S.K., Sudarshan, K., Pujari, P.K., 2021. Interpenetrating polymer network of rubbery epoxy and glassy PMMA: network inhomogeneities and dynamic heterogeneities. ACS Appl. Polym. Mater. 3, 5073–5086. https://doi.org/10.1021/acsapm.1c00825.

Sato, N., Murata, A., Fujie, T., Takeoka, S., 2016. Stretchable, adhesive and ultra-conformable elastomer thin films. Soft Matter 12, 9202–9209. https://doi.org/10.1039/C6SM01242F.

Sharp, J.S., Forrest, J.A., 2003. Free surfaces cause reductions in the glass transition temperature of thin polystyrene films. Phys. Rev. Lett. 91, 235701 https://doi.org/10.1103/PhysRevLett.91.235701.

Tada, H., Paris, P.C., Irwin, G.R., 2000. The Stress Analysis of Cracks Handbook, 3rd ed. ASME Press. https://doi.org/10.1115/1.801535.

Van Der Sanden, M.C.M., Meijer, H.E.H., Lemstra, P.J., 1993. Deformation and toughness of polymeric systems: 1. The concept of a critical thickness. Polymer (Guildf) 34, 2148–2154. https://doi.org/10.1016/0032-3861(93)90743-T.

Velez, N.R., Allen, F.I., Jones, M.A., Govindjee, S., Meyers, G.F., Minor, A.M., 2020. Extreme ductility in freestanding polystyrene thin films. Macromolecules 53, 8650–8662. https://doi.org/10.1021/acs.macromol.0c01387.

Wang, S.Q., Cheng, S., Lin, P., Li, X., 2014. A phenomenological molecular model for yielding and brittle-ductile transition of polymer glasses. J. Chem. Phys. 141, 094905 https://doi.org/10.1063/1.4893765.

Zhang, G., Kim, J., Hassan, S., Suo, Z., 2022. Self-assembled nanocomposites of high water content and load-bearing capacity. Proc. Natl. Acad. Sci. U. S. A. 119, e2203962119 https://doi.org/10.1073/pnas.2203962119.